

1 **Root responses to different types of TiO<sub>2</sub> nanoparticles and bulk counterpart in plant**  
2 **model system *Vicia faba* L.**

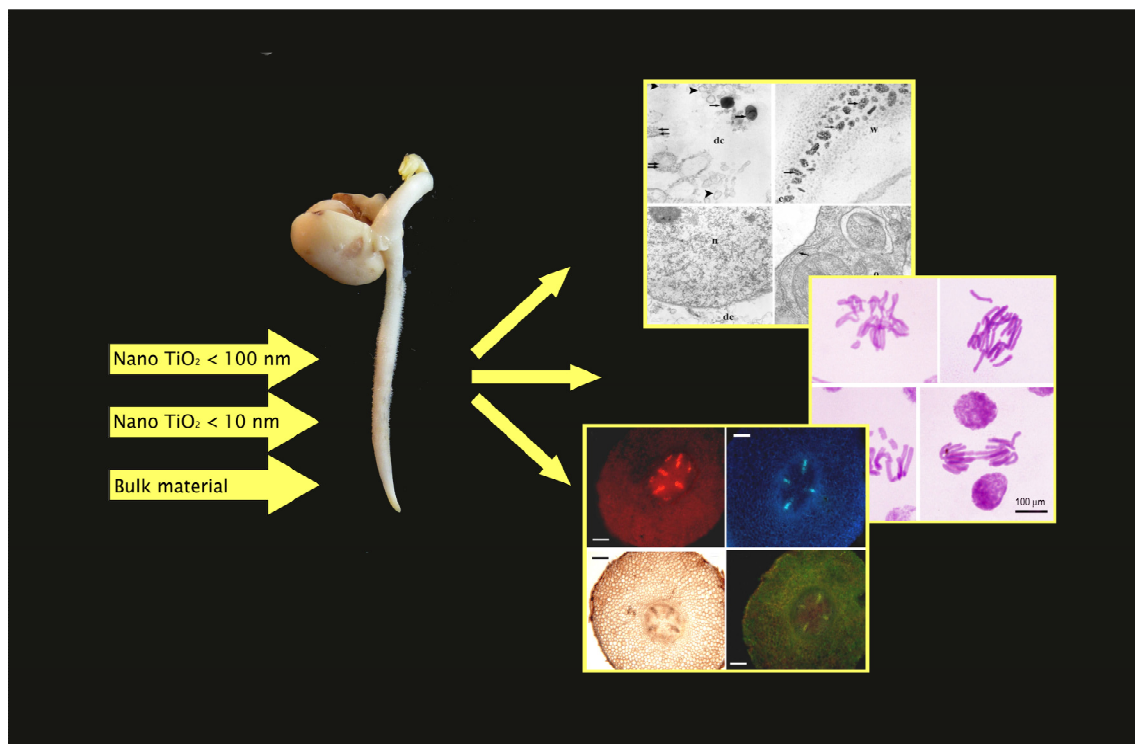
3

4 Monica Ruffini Castiglione<sup>1\*</sup>, Lucia Giorgetti<sup>2</sup>, Lorenza Bellani<sup>2,3</sup>, Simonetta Muccifora<sup>3</sup>, Stefania Bottega<sup>1</sup>,  
5 Carmelina Spanò<sup>1</sup>

6

7 <sup>1</sup>Department of Biology, University of Pisa, Via Ghini 13, 56126 Pisa, Italy; <sup>2</sup>Institute of Agricultural Biology  
8 and Biotechnology, UOS Pisa, CNR, Via Moruzzi 1, 56124 Pisa, Italy; <sup>3</sup>Department of Life Sciences, University  
9 of Siena, Via A. Moro 2, 53100 Siena, Italy

10



11

12 \*Corresponding author: [monica.ruffini.castiglione@unipi.it](mailto:monica.ruffini.castiglione@unipi.it), tel. +390502211317

13 All the authors contributed equally to the article

14

15 **Abstract**

16 The aim of the present work was to study , in the model system *Vicia faba* L., the potential  
17 stress-induced response to a commercial source of TiO<sub>2</sub> nanoparticles (NPs) <100nm  
18 (tetragonal crystals), to a TiO<sub>2</sub>-NPs laboratory-made sample <10nm (spherical shape), and to  
19 the corresponding bulk material, recently classified as possibly carcinogenic to humans.

20 The above materials were applied to *V. faba* seeds up to early seedling development; different  
21 endpoints were considered to estimate possible phytotoxic and genotoxic effects at  
22 ultrastructural, cyto-histological and physiological level. Oxidative stress and antioxidant  
23 response were evaluated by biochemical approach and *in situ* histochemical techniques.

24 Ultrastructural studies demonstrated that the applied NPs were internalized in root plant cells  
25 but the most damages to the cellular appearance followed bulk material treatment. Our results  
26 on seed vigor index, on aberration index, on the evaluation of oxidative stress and of induced  
27 antioxidant response demonstrated that TiO<sub>2</sub>-NPs may exert specific actions at different levels  
28 of toxicity, depending on their size and shape and that the bulk counterpart seems to provoke  
29 the major adverse effects in *V. faba* root.

30

31

32

33

34

35

36

37

38 *Keywords:* bulk material, faba bean, genotoxicity, oxidative stress, titanium dioxide

39 nanoparticles, ultrastructural studies

40        **1. Introduction**

41

42        Nanotechnologies are a tremendous opportunity for their positive impact in many sectors  
43 of economy, in industrial applications and in scientific research, but with unavoidable  
44 environmental emission and release of new chemicals. Nanoparticles (NPs) find their way  
45 into aquatic, terrestrial and atmosphere environments, where their fate and behaviour depend  
46 on the particle type, on their aggregation tendency and on bioavailability (Hotze et al., 2010).  
47 Therefore plants, organisms that strongly interact with their immediate environment, are  
48 expected to be affected by their exposition to NPs. As a consequence NPs have been recently  
49 included among the emerging contaminants by USEPA (2010). From the first decade of two  
50 thousand the first papers published on the potential effects of NPs on higher plants (Ma et al.,  
51 2010; Navarro et al., 2008; Ruffini Castiglione and Cremonini, 2009) evidenced some crucial  
52 points:

- 53 a) NPs, strongly enhancing or modifying the properties of the bulk materials, can interact in a  
54 non-predictable way with the environment and the living organisms;
- 55 b) NPs can explicate their actions depending on both the chemical composition and on the  
56 size and/or shape of the particles themselves;
- 57 c) NPs effects depend on the plant organism considered and on the variety of endpoints  
58 employed, sometimes making difficult comparative studies. In addition, the evaluation of  
59 specific effects, although fundamental to the understanding of the toxicity mechanisms,  
60 cannot be extended to all plant systems.

61        In the light of these considerations we can emphasize that the studies conducted so far on  
62 the phytotoxicity of NPs have produced data inadequate to characterize unambiguously their  
63 actions on plants, although many results demonstrate effects on *in vitro* cell culture,

64 embryogenesis, growth, biochemical processes and gene expression (Giorgetti et al., 2011;  
65 Kaveh et al., 2013; Poborilova et al., 2013).

66 TiO<sub>2</sub>-NPs, for their high stability, anticorrosive properties, redox selectivity, low production  
67 costs and their wide spectrum of new applications, are among the top five NPs used in  
68 consumer products (Chuankrerkkul and Sangsuk, 2008). Most of NPs applications are related  
69 to their characteristics of white pigment, four million tons being consumed annually  
70 worldwide (Ortlieb, 2010). Furthermore TiO<sub>2</sub>-NPs are widely used in common products  
71 (toothpastes, sunscreens, cosmetics, food products), in specific fields of medicines and  
72 pharmaceuticals, in certain sectors of agriculture and in environmental cleanup technologies  
73 (Bhawana and Fulekar, 2012; Liu, 2011).

74 Previous studies evidenced both positive and negative effects of TiO<sub>2</sub>-NPs on plants. Part  
75 of the scientific literature reports their significant improvement of germination, of shoot and  
76 root growth, of chlorophyll content, of transpiration and of water use efficiency (Raliya et al.,  
77 2015; Seeger et al., 2009; Song et al., 2013; Zheng et al., 2005). On the contrary, other papers  
78 report that plants can be harmed by TiO<sub>2</sub>-NPs with decrease in biomass, delayed germination,  
79 influence on mitotic index and genotoxic effects (Du et al., 2011; Ruffini Castiglione et al.,  
80 2011), DNA fragmentation, reactive oxygen species (ROS) production (Ghosh et al., 2010;  
81 Ruffini Castiglione et al., 2014) and changes in micro-RNA expression (Frazier et al., 2014).

82 The experimental design of this work was scheduled to study the potential effects of TiO<sub>2</sub>-  
83 NPs in the model system *Vicia faba*, at 72 h of seed germination, the most widely used  
84 treatment time assessing chemical-induced acute adverse effects (Baderna et al., 2015).

85 We choosed a middle-low exposure concentration that possibly might reproduce an actual  
86 environmental exposure, estimated by recent probabilistic material-flow modelling studies  
87 (Praetorius et al., 2012). On the basis of previous data showing negative effects only induced  
88 by high TiO<sub>2</sub> NPs concentrations (Ruffini Castiglione et al., 2014), we hypothesized plant

89 responses, not necessarily associated to toxic effects.

90 We employed two types of TiO<sub>2</sub>-NPs to assess if different responses in function of  
91 different particle size and characteristics were elicited. In addition, as corresponding bulk  
92 material, considered for decades an inert and safe material has been recently classified as  
93 possibly carcinogenic to humans (Group 2B carcinogen, IARC 2010), we tested also the  
94 effects of the same concentration of this form. To evaluate the hypothesized effects of these  
95 materials on *V. faba* seeds, we considered different cytological, physiological, histochemical  
96 and biochemical endpoints. Given that NPs can influence plant growth and development  
97 directly entering plant cells by means of different penetration mechanisms (Chichiriccò and  
98 Poma, 2015) or even without being internalized, a further aim of our work was to understand  
99 how these materials can affect *V. faba* root ultrastructure in function of the shape and of the  
100 size of the NPs.

101

## 102 **2. Materials and methods**

### 103 *2.1. Seed germination and seedling development*

104 Seeds of *Vicia faba* L. var. *minor* were washed over night in tap water, germinated at 24±1  
105 °C for 72 h in the dark in Petri dishes in water (control, sample C), in a suspension of two  
106 rutile/anatase TiO<sub>2</sub>-NPs: < 100 nm (sample S: tetragonal crystals, from Sigma-Aldrich, USA);  
107 < 10 nm (sample P: spherical shape, produced by pulsed laser ablation in liquids) (Giorgetti et  
108 al., 2014), kindly provided by PlasmaTech, Pisa (Italy) and in bulk TiO<sub>2</sub> (sample B, from  
109 Sigma-Aldrich, USA). All the treatments were performed at the selected concentration of 50  
110 mg/L. For all treatments 5 Petri dishes with 10 seeds each were set up. Three days after  
111 treatment, the germination percentage and the seedling root length were evaluated in all  
112 samples.

113 Vigour index (VI) was calculated with the following formula:

114 VI = Germination (%) x Seedling Growth (mm).

115 Roots were collected for cytological, histochemical and biochemical determinations as  
116 described below.

117

### 118 2.2. *Transmission electron microscope (TEM)*

119 To evaluate morphology and size of the different TiO<sub>2</sub>-NPs, a drop (10 µL, 50 mg/L) of  
120 samples S and P was placed on TEM grids covered with formvar, allowed to settle and dry.

121 For TEM root observations, small cubes of control and treated roots were pre-fixed in  
122 Karnovsky solution (Karnovsky, 1965), post-fixed in osmium tetroxide, dehydrated and  
123 embedded in Epon 812-Araldite A/M mixture. Thin sections were stained with uranyl acetate  
124 and lead citrate.

125 Isolated NPs and root sections were observed under a FEI Tecnai G2 Spirit electron  
126 microscope at 100 kv.

127

### 128 2.3. *Cytological studies on root meristem*

129 Ten roots for each treatment were fixed in ethanol: glacial acetic acid (3:1 v/v) for 12 h.  
130 Root tips were squashed and stained following Feulgen technique (Giorgetti and Ruffini  
131 Castiglione, 2016).

132 At least 1000 nuclei, randomly selected for each slide, were analyzed by light microscope.

133 Perturbations in mitotic activity (mitotic index, MI, = number of mitosis/100 nuclei)  
134 indicate cytotoxicity, while both micronuclei presence (MNC=Micronucleus frequency/1000  
135 nuclei) and mitotic aberrations (aberration index, AI, = number of aberrations/100 nuclei)  
136 indicate the genotoxicity of a treatment. The scored aberrations included chromosomal  
137 bridges, fragments, lagging chromosomes, stickiness, aberrant metaphases and disturbed  
138 anaphases in dividing cells, micronuclei in interphase cells (Ruffini Castiglione et al., 2011).

139 2.4. *Histochemical detection of oxidative stress on root system*

140 Five roots for each treatment were hand sectioned in correspondence to the initial root hair  
141 area. Cross sections were immediately processed with specific staining reagents for  
142 fluorescence and optical microscopy. Fluorescence microscope analysis was carried out with a  
143 Leica DMLB, equipped with appropriate set of excitation/emission filters and with a Leica  
144 DC300 ccd camera; optical microscope analysis was performed with a Leitz Diaplan,  
145 equipped with a Leica DCF420 ccd camera. Fluorescent Amplex Ultrared® (Life  
146 Technologies, USA) was applied for *in situ* detection of hydrogen peroxide (H<sub>2</sub>O<sub>2</sub>) following  
147 manufacturing instructions. In brief, sections were incubated for 30 min at room temperature  
148 (RT) in the dark in the staining mixture composed by 50 µl of 10mM Amplex Ultrared stock  
149 solution in DMSO, 100 µl horseradish peroxidase (Sigma-Aldrich, USA) (10 U/ml in 0.05M  
150 PB, pH 6), 4.85 ml of 0.05M PB pH 6. After three washes in the same buffer, the slices were  
151 mounted in glycerol and observed with fluorescence microscope (568<sub>ex</sub>/681<sub>em</sub> nm). Reactive  
152 nitrogen species (RNS) were revealed by 2,3-Diaminonaphthalene staining (Life  
153 Technologies, USA) dissolved in DMSO (0.5M) and then diluted 1:1000 in PBS 0.05M pH  
154 6.8 just before the sample incubation in the dark at RT. After 30 min and three washes in the  
155 same buffer, slices were mounted in glycerol for the observations with fluorescence  
156 microscope (365<sub>ex</sub>/415<sub>em</sub> nm). BODIPY® 581/591 C11 was used as free radical sensor to  
157 visualize lipid peroxidation levels as a change of the fluorescence emission peak from red to  
158 green. The slices were incubated in 10 µM BODIPY in PBS 0.1M pH 7.4 for 30 min at RT in  
159 the dark and then washed three times in the same buffer. Microscope evaluation was  
160 performed acquiring simultaneously the green (485<sub>ex</sub>/510<sub>em</sub> nm) and the red fluorescence  
161 (581<sub>ex</sub>/591<sub>em</sub> nm) signals and merging the two images (Kováčik et al., 2014). Endogenous  
162 peroxidase activity was visualized under optical microscope exploiting a solution of  
163 colourless guaiacol/H<sub>2</sub>O<sub>2</sub> (5mM H<sub>2</sub>O<sub>2</sub>, 5mM guaiacol in 60mM PB pH 6.1) that became

164 dark/brown tetraguaiacol, due to peroxidase activity. After 10 min of incubation the slices  
165 were washed three times in the same buffer and mounted in glycerol for microscope analysis  
166 (Lepeduš et al., 2005).

167

#### 168 *2.5. Determination of water content (WC) and of relative water content (RWC)*

169 Fresh weight (FW) was obtained by weighing the fresh roots. The roots were then  
170 immersed in water overnight (turgid weight, TW), oven-dried at 100°C to constant weight  
171 and reweighed (dry weight, DW).

172 WC percentage was estimated on the FW basis. RWC was determined as in Balestri et al.  
173 (2014) and calculated with the formula:

$$174 \text{ RWC} = [(\text{FW}-\text{DW})/(\text{TW}-\text{DW})] \times 100$$

175

#### 176 *2.6. Extraction and determination of H<sub>2</sub>O<sub>2</sub> and thiobarbituric acid reactive substances* 177 *(TBARS)*

178 H<sub>2</sub>O<sub>2</sub> content of roots was determined according to Jana and Choudhuri (1982). Roots  
179 were ground and homogenised with phosphate buffer 50mM pH 6.5. The homogenate was  
180 centrifuged at 6000g for 25 min. H<sub>2</sub>O<sub>2</sub> content was determined using 0.1% titanium  
181 chloride in 20% (v/v) H<sub>2</sub>SO<sub>4</sub>. The amount of H<sub>2</sub>O<sub>2</sub> was detected spectrophotometrically  
182 (410 nm), calculated from a standard curve and expressed as μmol g<sup>-1</sup>DW.

183 Lipid peroxidation in roots was measured determining the amount of TBARS by the  
184 thiobarbituric acid (TBA) reaction (Hartley-Whitaker et al., 2001) with minor  
185 modifications. Roots were mixed with TBA reagent (10% w/v trichloroacetic acid + 0.25%  
186 w/v thiobarbituric acid), heated (95°C for 30 min), cooled for 15 min and centrifuged at  
187 2000g for 15 min. The level of TBARS was detected as specific absorbance at 532 nm by  
188 subtracting the non-specific absorbance at 600 nm and calculated using an extinction



189 coefficient of  $155\text{mM}^{-1}\text{cm}^{-1}$ . TBARS were expressed in  $\text{nmol g}^{-1}\text{DW}$ .

190

### 191 *2.7. Extraction and determination of proline*

192 Proline concentration was determined according to Bates (1973) with minor  
193 modifications (Spanò et al., 2013). Root were homogenised with 3% sulfosalicylic acid.  
194 The supernatant was incubated with glacial acetic acid and ninhydrin reagent (1:1:1) and  
195 boiled at  $100^{\circ}\text{C}$  for 60 min. After cooling the reaction mixture, toluene was added and the  
196 absorbance of toluene phase was read at 520 nm. Calculations were made on the base of a  
197 standard curve and content was expressed as  $\mu\text{mol g}^{-1}\text{DW}$ .

198

### 199 *2.8. Extraction and determination of ascorbate and glutathione*

200 Ascorbate, reduced form (ASA) and oxidised form (dehydroascorbate, DHA), extraction  
201 and determination were performed according to Spanò et al. (2011). Calculations were  
202 made on the base of a standard curve. A blank was made in the absence of the extract and  
203 content was expressed as  $\mu\text{mol g}^{-1}\text{DW}$ .

204 Glutathione was extracted and determined according to Gossett et al. (1994). Total  
205 glutathione (reduced form, GSH + oxidised form, GSSG) was detected monitoring the rate  
206 of change in absorbance at 412 nm. GSSG was determined after removal of GSH from the  
207 extract by 2-vinylpyridine derivatization. GSH was detected by subtracting the amount of  
208 GSSG from total glutathione and calculations were made on the base of a standard curve. A  
209 blank was made in the absence of the extract and content was expressed as  $\mu\text{mol g}^{-1}\text{DW}$ .

210

### 211 *2.9. Enzyme extraction and assays*

212 Roots were ground in liquid nitrogen and the extraction was made at  $4^{\circ}\text{C}$  as in Spanò et  
213 al. (2013). The homogenate was then centrifuged at  $15000g$  for 20 min. For ascorbate

214 peroxidase, 2mM ascorbate was added to the extraction medium. Supernatants were  
215 collected and stored in liquid nitrogen until their use for enzymatic assays.

216 Ascorbate peroxidase (APX, EC 1.11.1.11) activity was measured according to Nakano  
217 & Asada (1981). Enzyme activity was assayed from the decrease in absorbance at 290 nm  
218 (extinction coefficient  $2.8\text{mM}^{-1}\text{cm}^{-1}$ ) as ascorbate was oxidised and enzyme extract  
219 contained  $25\ \mu\text{g protein ml}^{-1}$ . Correction was made for the low, non-enzymatic oxidation of  
220 ascorbate by  $\text{H}_2\text{O}_2$  (blank).

221 Glutathione peroxidase (GPX, EC 1.11.1.9) activity was determined according to  
222 Navari-Izzo et al. (1997) following the oxidation of NADPH at 340 nm (extinction  
223 coefficient  $6.2\ \text{mm}^{-1}\ \text{cm}^{-1}$ ). Enzymatic extract contained  $12.5\ \mu\text{g protein ml}^{-1}$ .

224 Catalase (CAT, EC 1.11.1.6) activity was determined according to Aebi (1984).  
225 Enzymatic extract contained  $12.5\ \mu\text{g protein ml}^{-1}$ . A blank containing only the enzymatic  
226 solution was made. Specific activity was calculated from the  $39.4\text{mM}^{-1}\ \text{cm}^{-1}$  extinction  
227 coefficient.

228 Guaiacol peroxidase (POD, EC 1.11.1.7) activity was determined according to Arezky  
229 et al. (2001) using 1% guaiacol as substrate. Enzymatic extract contained  $5\ \mu\text{g protein ml}^{-1}$ .  
230 Enzymatic activity was determined following guaiacol oxidation by  $\text{H}_2\text{O}_2$  (extinction  
231 coefficient  $26.6\text{mM}^{-1}\ \text{cm}^{-1}$ ) at 470 nm, one unit oxidising  $1.0\ \mu\text{mole}$  guaiacol per min.

232 All enzymatic activities were determined at  $25^\circ\text{C}$  and expressed as  $\text{U g}^{-1}$  protein. Protein  
233 measurement was performed according to Bradford (1976), using BSA as standard.

234

### 235 *2.10. Statistical analysis*

236 All the data were the mean of at least three replicates from three independent experiments.  
237 Statistical significance was determined by ANOVA tests followed by *post hoc* Bonferroni  
238 multiple comparison test. *Post hoc* statistical significance is indicated in figures and tables

239 by different letters.

240

### 241 **3. Results**

#### 242 *3.1. Germination and growth*

243 Germination percentage (Table 1) did not show significant differences between control  
244 and treated materials. After 72 h germination roots from B treated seeds were significantly  
245 shorter than P-NPs treated roots but not significantly different from C and S-NPs treated  
246 materials (Fig. 1, Table 1). The highest VI (Table 1) was detected in P-NPs treated roots,  
247 while the minimum value was characteristic of B treated samples.

248

#### 249 *3.2. TEM observations*

250 The morphology of the TiO<sub>2</sub> P and S-NPs is shown in Figs 2a and 2b, respectively. Both  
251 were extremely variable in electron density (Figs 2a, b). P-NPs were roughly round in shape  
252 with a diameter from 2 to 12 nm (Fig. 2a). S-NPs had polyhedral shape and a wide size  
253 distribution ranging from 10 to 100 nm (Fig. 2b). Sections of control roots showed cells with  
254 large vacuoles with scanty materials evident. The cytoplasm was rich in well structured  
255 organelles, particularly long rough endoplasmic reticulum cisternae, dictyosomes,  
256 mitochondria and plastids (Fig. 2c). The cell ultrastructure of P-NPs treated roots appeared  
257 similar to control ones. The only noteworthy difference was the presence of electron dense  
258 particles embedded in scanty electron dense material scattered in the cell vacuole (Fig. 2d).  
259 Often dense particles of 5-12 nm were observed crossing the walls of rhizodermis and of root  
260 parenchyma cells (Figs 2e, f).

261 The S-NPs treated roots showed cell vacuoles containing single or aggregated NPs (Fig.  
262 3a). Several cells showed wide zone of cytoplasmic degeneration (Fig. 3b) often surrounded  
263 by a double membrane. In these cytoplasmic portions a large number of small and/or large

264 vesicles with rough membranes and NPs of polyedric form, isolated or aggregated, were  
265 observed (Fig. 3b). Some of these cells showed more or less evident plasmalemma-wall  
266 detachment as in plasmolysis (data not shown). In the cell walls of rhizodermis numerous  
267 aggregates (60-120 nm) of dense particles were often present (Fig. 3c). Numerous vesicles,  
268 smooth endoplasmic reticulum cisternae and organelles, often not well recognizable, were  
269 present in the cells of the B treated roots (Fig. 3d). Some cells showed nuclei with extremely  
270 disperse chromatin and wide portion of cytoplasmic degeneration (Fig. 3e). Furthermore, a  
271 great number of cells evidenced an amazing electron dense cytoplasm with numerous not well  
272 recognizable organelles (probably plastids), amyloplasts and weakly electron opaque bodies  
273 of about 0.3- 0.5  $\mu\text{m}$  in diameter (Fig. 3f).

274

### 275 *3.3. Cytological evaluation of the root meristem*

276 The mitotic activity (MI) and the occurrence of micronuclei in interphase (MNC),  
277 evidenced not significant disturbances under different treatments. On the contrary, when the  
278 frequency of anomalies and/or aberrations (AI) in dividing cells were recorded, a significant  
279 increase in the AI was observed for the samples S and B, while the mean value of the AI in  
280 the samples P was not statistically different from the control (Fig. 4). Fig. 5 shows some  
281 representatives examples of the scored mitotic abnormalities.

282

### 283 *3.4. Histological evaluation associated to in situ detection of oxidative stress*

284 Probes specific for  $\text{H}_2\text{O}_2$ , RNS, lipid peroxidation and guaiacol-peroxidase activity (Fig. 6)  
285 directly detect qualitative signals related to oxidative stress. In cross sections of control and  
286 treated roots the signal obtained with the fluorescent probe Amplex  $\text{H}_2\text{O}_2$ , apart from a faint  
287 staining involving the cortical area, was mainly localized in xylem vessels (Fig. 6a). In the  
288 samples treated with both the types of NPs we observed a general increase of  $\text{H}_2\text{O}_2$  in the

289 vascular cylinder involving as well the phloem, alternated between the arms of the xylem  
290 (Figs 6b, c). On the contrary, the roots treated with bulk material showed a strong staining in  
291 the rhizodermis and in the periphery of the cortical cylinder (Fig. 6d).

292 Concerning the RNS, the control root presented a distinctive blue staining involving  
293 mainly the xylem vessels, and, to a lesser extent, the region surrounding the stele and the  
294 peripheral area of the cortex (Fig. 6e). Under treatments, we observed a general increase of  
295 the fluorescence intensity in respect to the control, especially in the samples S and B (Figs 6f,  
296 g, h). Sample B was the most reactive also at the BODIPY fluorescent probe (Fig. 6l), which  
297 identified lipid peroxidation as a change of the fluorescence emission peak from red to green.  
298 In this sample the green fluorescence was observed in all the root tissues, with the exception  
299 of the central part of the stele. Samples P and S (Figs 6j, k) were similar to the control (Fig.  
300 6i) as to the intensity of the staining in the root cortex, but a well defined green area  
301 corresponding to the perycicle and to the outermost cells of vascular tissues was observed in  
302 sample S (Fig. 6k). Figs 6m-p shows representative sections after guaiacol staining. The  
303 brown colour indicates peroxidase activity induced by treatments. Root cross sections were  
304 lightly stained in samples C and P (Figs 6m, n), the former showing a more diffuse signal, the  
305 latter being more sharply stained, also in the area of phloem arcs. Guaiacol reaction strongly  
306 increased in the S and B samples (Figs 6o, p).

307

### 308 *3.5. Water content and relative water content*

309 Bulk-treated material was characterized by the highest values of both WC and RWC (Table  
310 1). Roots of NPs-treated samples, on the other hand, showed all similar hydric status.

311

### 312 *3.6. H<sub>2</sub>O<sub>2</sub> and TBARS*

313 The highest contents of H<sub>2</sub>O<sub>2</sub> and TBARS (Table 1) were detected in B roots. H<sub>2</sub>O<sub>2</sub>

314 concentration was lower in C roots and even more in S samples, showing the lowest value in  
315 P-NPs treated material. Both NPs-treated roots had TBARS content not significantly different  
316 from C roots.

317

### 318 *3.7. Proline and low molecular weight antioxidants*

319 Proline (Table 1) had the highest value in C roots, was significantly lower in B and even  
320 more in NPs-treated seeds, regardless of the type of NPs used. B roots were characterized by  
321 the highest contents of both total ascorbate and glutathione (Table 1). P-NPs treated roots  
322 showed the lowest values of these low molecular weight antioxidants, while S roots did not  
323 differ significantly from control material. Interestingly, the highest values of reducing power  
324 of ASA/DHA couples were characteristic of NPs-treated roots. Significantly high was the  
325 GSH/GSSG ratio in sample P (Table 1).

326

### 327 *3.8. Antioxidant enzymes*

328 Although no significant difference was observed in GPX activity among different  
329 treatments, both APX and CAT activities were significantly lower in all treated roots,  
330 regardless of the type of treatment (Table 1). The highest POD activity was detected in S-NPs  
331 treated roots, significantly lower values in B then in C samples and the lowest activity in P-  
332 NPs treated samples.

333

## 334 **4. Discussion**

335 NPs can influence plant growth and development without being internalized (Asli and  
336 Neumann, 2009) or directly entering plant cells by means of different penetration mechanisms  
337 (Chichiriccò and Poma, 2015), also when they have dimensions higher than cell wall pore  
338 exclusion limit (Larue et al., 2012). However, few literature data are available concerning the

339 effects of TiO<sub>2</sub>-NPs and bulk material on root ultrastructure. The present ultrastructural  
340 observations confirmed the presence of TiO<sub>2</sub>-NPs inside *V. faba* root cells and provided  
341 significant information on their effects. The NPs penetrated through the cell walls of  
342 rhizodermis and moved via the apoplast pathway. Indeed they were observed in the P-NPs  
343 treated root wall generally as individual particles, while the S-NPs crossed the rhizodermis  
344 walls as aggregates. The wall pore size can allow the diffusion of molecules (exceptionally)  
345 up to 10 nm of diameter (Larue et al., 2012), as a consequence the P-NPs can cross the  
346 rhizodermis and move through the apoplasm. It was supposed a NPs induction of hydroxyl  
347 radicals that can loose the wall with enlargement of pores by cleavage of pectin-  
348 polysaccharides (Kim et al., 2014; Larue et al., 2012). In this way it is possible to explain the  
349 wall penetration of the large particles and of S-NPs aggregates. The vacuolar sequestration of  
350 P-NPs allows to avoid interaction of particles with organelles and metabolic process. The  
351 success of this detoxification mechanism is attested by the fact that the cell ultrastructure of  
352 P-NPs treated roots appeared similar to the control ones. On the contrary, in S-NPs treated  
353 roots the NPs were localized both in the vacuoles and in wide zones of degenerated  
354 cytoplasm, often surrounded by a double membrane. These findings recall the double  
355 membrane autophagosomes that form in response to biotic and abiotic stress and can bring to  
356 programmed cell death (Kutik et al., 2014). This process is characterized by gradual lysis of  
357 the cellular content leaving at the end the hollow cell wall shell (Kutik et al., 2014).  
358 Therefore, in *V. faba* the damage of the cell ultrastructure appeared to be related to size and  
359 shape of NPs. B treatment strongly affected cell ultrastructure, as electron dense cytoplasm  
360 and numerous not well recognizable organelles (probably plastids), amyloplasts, and weakly  
361 electron opaque bodies of about 0.3-0.5 µm diameter were observed, giving the appearance of  
362 not yet differentiated embryo cells.

363         Contrasting results were reported about the effects of TiO<sub>2</sub>-NPs on plant germination and

364 growth (Ghosh et al., 2010; Ruffini Castiglione et al., 2011, 2014; Seeger et al., 2009; Song et  
365 al., 2013). In *V. faba* the different treatments of TiO<sub>2</sub>-NPs and bulk material did not cause  
366 germination inhibition, but bulk material induced the production of seedlings with the shortest  
367 roots. This is in contrast with Azimi et al. (2013) who reported no variation in root length in  
368 seeds of *Agropyron desertorum* treated with similar concentrations of bulk TiO<sub>2</sub>. Additional  
369 interesting information can derive from VI, which, summarizing the impact of a particular  
370 compound on seed germination and seedling growth, can give an idea of the whole  
371 germination process (Ruffini Castiglione et al., 2014). Our previous data on another species of  
372 *Vicia* revealed a phytotoxic effect only at the highest (4‰) S-NPs concentration. In  
373 accordance, *V. faba* treated with low concentrations of S-NPs had a VI comparable with that  
374 of C material. The increase in VI induced by P-NPs was in accordance with reports by Feizi et  
375 al. (2013) for sage underlining a different action of NPs in function of the size and shape.  
376 Despite the minor root growth, B-treated plants were characterized by a good hydric status, as  
377 indicated by WC and RWC, showing that the impaired root growth was not due to tissue  
378 water deficit.

379 DNA injuries and genotoxic effects were demonstrated after TiO<sub>2</sub>-NPs treatments both in  
380 animal (Shukla et al., 2013) and in plant systems (Ghosh et al., 2010; Ruffini Castiglione et  
381 al., 2011, 2014; Moreno-Olivas et al., 2014; Pakrashi et al., 2014) by different experimental  
382 approaches such as comet assay, chromosomal aberration analysis, micronuclei assay,  $\gamma$ -  
383 H2AX assay, DNA laddering assay and RAPD analysis.

384 Concerning cytological evaluation of the root meristem behaviour, in contrast to what was  
385 observed in the root apex following plant treatments with nano- and macroscale metals  
386 (Kumari et al., 2009; Balestri et al., 2014), no negative effect was registered for the mitotic  
387 activity in our experimental conditions: all the recorded MI were not significantly different  
388 from the control, indicating absence of cytotoxicity for all the treatments. Also the MNC,



389 recently standardized for *V. faba* by an international protocol, ISO 29200 (Cotelle et al.,  
390 2015), did not reveal toxic effects on root apex. In this plant system, the absence of  
391 micronuclei induction occurred in parallel with an increase in the frequency of AI in samples  
392 S and B. The lack of concordance between MNC test and AI in these two treatments indicated  
393 that S-NPs and the bulk counterpart could act as indirect toxicants and/or exert on  
394 meristematic cells a delayed effect along 72 hours of treatment, allowing to detect only  
395 anomalies and/or aberrations in dividing cells but not the resulting micronuclei in the  
396 subsequent interphase. Genotoxic effects of S-NPs were already observed on *V. narbonensis*  
397 and *Zea mays* (Ruffini Castiglione et al., 2011) at higher concentrations (200-4000 mg/L);  
398 besides bulk material provoked a genotoxic response in *Allium cepa* at about 100 mg/L and  
399 above (Ghosh et al., 2010).

400 The genotoxicity of NPs, supposed to be due to oxidative stress as the primary key  
401 mechanism inducing DNA damages, strongly coupled to ROS activity and to depletion of cell  
402 antioxidant response. ROS, such as superoxide, H<sub>2</sub>O<sub>2</sub> and hydroxyl radicals may act as  
403 elicitors of common stress response (Mittler, 2002); however when they accumulate at critical  
404 level an oxidative stress can ensue (Parida and Das, 2005). Nevertheless, H<sub>2</sub>O<sub>2</sub> may act as an  
405 active regulator of biological processes related to growth and differentiation (Bellani et al.,  
406 2012), as observed in tracheary elements and in endodermis of the control and all the treated  
407 samples.

408 Previous studies showed that NPs can induce both increase (Zhao et al., 2012) and  
409 decrease (Sharma et al., 2012) in H<sub>2</sub>O<sub>2</sub> content, even in the same species in a NPs  
410 concentration-dependent manner (Ruffini Castiglione et al., 2014). In our experimental  
411 conditions, in accordance with data on *Cicer arietinum* (Mohammadi et al., 2014), TiO<sub>2</sub>-NPs  
412 induced a significant decrease in the content of this molecule, the lowest value characterizing  
413 P-NPs treated roots. The low H<sub>2</sub>O<sub>2</sub> content for P and S-NPs treated materials could be due at

414 least in part to a possible radical scavenging activity of TiO<sub>2</sub>-NPs, higher at the decrease in  
415 particle size and increase in surface area (Kalyanasundharam and Prakash, 2015). This  
416 scavenging role could be very helpful in increasing plant tolerance under stress condition  
417 (Mohammadi et al., 2014). Roots treated with P and S-NPs showed a peculiar staining pattern  
418 of H<sub>2</sub>O<sub>2</sub> in different root compartments, involving mainly the vascular cylinder and the  
419 phloem arcs: this H<sub>2</sub>O<sub>2</sub> localization may be allied to a different root response elicited by the  
420 nanomaterials. The highest content of H<sub>2</sub>O<sub>2</sub> was detected in the rhizodermis and in the  
421 peripheral cortex of bulk-treated seedlings. This could be related to lignification processes as  
422 resistance mechanism promoting plant defence (Moura et al., 2010).

423 With histochemical approach, lipid peroxidation was strongly and diffusely detectable in  
424 B treated samples, as confirmed by TBARS assay, indicative of membrane damage, mainly in  
425 root cortex. In this material the good correlation between TBARS and H<sub>2</sub>O<sub>2</sub> content could  
426 indicate an H<sub>2</sub>O<sub>2</sub>-dependent membrane damage. These data are in line with ultrastructural  
427 observations on B treated samples. NPs treatments induced, in accordance with biochemical  
428 data, a whole signal comparable to the control, apart from a peculiar staining pattern in the  
429 outermost layers of vascular cylinder characteristics for the S-NPs. The lack of membrane  
430 damage in NPs-treated materials and C roots is in accordance with previous data on *V.*  
431 *narbonensis* treated with higher S-NPs concentrations (Ruffini Castiglione et al., 2014).  
432 Therefore, *V. faba* root seems to be strongly harmed by bulk material treatment while TiO<sub>2</sub> S-  
433 NPs may act inducing a localized tissue-specific membrane damage. To protect cellular  
434 structure and metabolism from oxidative damage, plant evolved a complex enzymatic and non  
435 enzymatic system. Proline can contribute along with ascorbate and glutathione to ROS  
436 detoxification. Given the lower proline content in treated seedlings than in control ones, the  
437 main antioxidant roles were played in our conditions by ascorbate and glutathione in  
438 accordance with literature (Jiang et al., 2014). The higher pools of both ascorbate and

439 glutathione in bulk-treated material showed the importance of these antioxidants in oxidative  
440 stress response. The highest reducing power recorded in NPs-treated roots was in line with the  
441 low H<sub>2</sub>O<sub>2</sub> content detected in these materials.

442 Enzymatic activities were generally inhibited in treated seedlings, with the exception of  
443 GPX characterized by similar activities in all materials. The decrease in CAT activity detected  
444 in NPs-treated roots was also relieved in onion seedlings treated with TiO<sub>2</sub>-NPs of size similar  
445 to that of our P material (Laware and Raskar, 2014) showing the particular sensitivity of this  
446 enzyme to TiO<sub>2</sub>-NPs. Our results highlighted a different POD activity in dependence from  
447 NPs size: in particular the maximum value was observed in S-treated roots, confirming  
448 previous data obtained in *V. narbonensis* under different concentrations of the same NPs  
449 (Ruffini Castiglione et al., 2014), while in P-NPs roots POD activity was lower than in control  
450 roots. These results were basically comparable to those obtained *in situ* by guaiacol-  
451 peroxidase staining, resembling the recorded pattern of H<sub>2</sub>O<sub>2</sub> staining with a specific  
452 involvement of the phloem tissues for the samples treated with both TiO<sub>2</sub>-NPs. Guaiacol  
453 peroxidase activity, known as having important roles in control of growth by lignification  
454 (Gaspar et al., 1991), was stronger in xylem vessels under all the treatments, indicating a  
455 precocious status of tracheary element differentiation in respect to the control. This process  
456 seems to be more pronounced in the treatments with S-NPs and B material as further  
457 confirmed by the localization of RNS, among which NO is involved as signal molecule, in  
458 plant cell differentiation, xylogenesis and cell wall lignification (Planchet and Kaiser, 2006).

459

## 460 **5. Conclusions**

461 On the whole, the low concentration of the different materials was able to induce specific  
462 responses in our plant model system. Germination process was stimulated in P-NPs treated  
463 seeds. TiO<sub>2</sub>, supplied as bulk material, induced oxidative stress, in terms of both H<sub>2</sub>O<sub>2</sub> and

464 TBARS content, disturbance in root growth and in cellular ultrastructure. Genotoxic effects,  
465 detectable in bulk treated roots, were however also evident following S-NPs treatment.  
466 In addition *in situ* analysis revealed localized stress signals in specific root compartments  
467 related to developmental and/or defence response, typical for the different treatments. In bulk-  
468 treated roots antioxidant defence seemed to rely mainly on low molecular weight  
469 antioxidants. In the different NPs-treatments a high reducing power of glutathione in P-NPs  
470 treated seedlings and a high POD activity in S-NPs treated material were observed. The  
471 activation of the antioxidant response in the presence of low levels of H<sub>2</sub>O<sub>2</sub> is particularly  
472 interesting as it could help to explain the protective action of TiO<sub>2</sub>-NPs in plants subjected to  
473 abiotic stress. These results all together suggest that TiO<sub>2</sub>-NPs, able to penetrate into root  
474 cells, may exert different actions depending on their size and their shape and that the bulk  
475 counterpart, in our experimental conditions, seems to provoke the major adverse effects in *V.*  
476 *faba* roots.

477

478

#### 479 **Acknowledgments**

480 Our special thanks go to Dr C. Vergari and Prof. F. Giammanco (Plasma Tech, Polo  
481 Tecnologico Navacchio, Pisa, Italy) for kindly providing P nanoparticles.

482 This work was supported by local funding of the University of Pisa (ex 60 %).

483 **References**

484

485 Aebi, H., 1984. Catalase *in vitro*. Meth. Enzym. 105, 121-126.

486 Arezky, O., Boxus, P., Kevers, C., Gaspar, T., 2001. Changes in peroxidase activity, and  
487 level of phenolic compounds during light-induced plantlet regeneration from  
488 *Eucalyptus camaldulensis* Dhen. nodes *in vitro*. Plant Growth Regul. 33, 215-219.

489 Asli, S., Neumann, P.M., 2009. Colloidal suspensions of clay or titanium dioxide  
490 nanoparticles can inhibit leaf growth and transpiration via physical effects on root  
491 water transport. Plant Cell Environ. 32, 577-584.

492 Azimi, R., Feizi, H., Khajeh Hosseini, M., 2013. Can bulk and nanosized titanium dioxide  
493 particles improve germination features of wheatgrass (*Agropyron desertorum*). Not.  
494 Sci. Biol. 5, 325-331.

495 Baderna, D., Lomazzi, E., Pogliaghi, A., Ciaccia G., Lodi M., Benfenati, E. 2015. Acute  
496 phytotoxicity of seven metals alone and in mixture: are Italian soil threshold  
497 concentrations suitable for plant protection? Environ. Res. 40, 102–111.

498 Balestri, M., Ceccarini, A., Forino L.M.C., Zelko, I., Martinka, M., Lux, A., Ruffini  
499 Castiglione, M., 2014. Cadmium uptake, localization and stress -induced morphogenic  
500 response in the fern *Pteris vittata*. Planta 239, 1055-1064.

501 Balestri, M., Bottega, S., Spanò, C., 2014. Response of *Pteris vittata* to different cadmium  
502 treatments. Acta Physiol. Plant. 36, 767-775.

503 Bates, L.S., 1973. Rapid determination of free proline for water-stress studies. Plant Soil  
504 39, 205-207.

505 Bellani, L.M., Salvini, L., Dell'Aquila, A., Scialabba, A., 2012. Reactive oxygen species  
506 release, vitamin E, fatty acid and phytosterol contents of artificially aged radish  
507 (*Raphanus sativus* L.) seeds during germination. Acta Physiol. Plant. 34, 1789-1799.

508 Bhawana, P., Fulekar, M.H., 2012. Nanotechnology: remediation technologies to clean up  
509 the environmental pollutants. Res. J. Chem. Sci. 2, 90-96.

510 Bradford, M., 1976. A rapid and sensitive method for the quantitation of microgram  
511 quantities of protein utilizing the principle of protein-dye binding. Anal. Biochem. 72,  
512 248-254.

513 Chichiriccò, G., Poma, A., 2015. Penetration and toxicity of nanomaterials in higher plants.  
514 Nanomaterials 5, 851-873.

515 Chuankrerkkul, N., Sangsuk, S., 2008. Current status of nanotechnology consumer  
516 products and nano-safety issues. J. Min. Met. Mat. Soc. 18, 75-79.

517 Cotelle, S., Dhyèvre, A., Muller, S., Chenon, P., Manier, N., Pandard, P., Echairi, A.,  
518 Silvestre, J., Guiresse, M., Pinelli, E., Giorgetti, L., Barbafieri, M., Engel, F., Radetski,  
519 C.M., 2015. Soil genotoxicity assessment-results of an interlaboratory study on the  
520 *Vicia* micronucleus assay in the context of ISO standardization. Environ. Sci. Pollut.  
521 Res. Int. 22, 988-995.

522 Du, W., Sun, Y., Ji, R., Zhu, J., Wu, J., Guo, H., 2011. TiO<sub>2</sub> and ZnO nanoparticles  
523 negatively affect wheat growth and soil enzyme activities in agricultural soil. J.  
524 Environ. Monit. 13, 822-828.

525 Feizi, H., Shahram, A., Farzin, A., Saeed, J.P., 2013. Comparative effects of nanosized and  
526 bulk titanium dioxide concentrations on medicinal plant *Salvia officinalis* L. Ann. Rev.  
527 Res. Biol. 3, 814-824.

528 Frazier, T.P., Burklew, C.E., Zhang, B., 2014. Titanium dioxide nanoparticles affect the  
529 growth and microRNA expression of tobacco (*Nicotiana tabacum*). Funct. Integr.  
530 Genomics 14, 75-83.

531 Gaspar, T.H., Penel, C., Hagege, D., Greppin, H., 1991. Peroxidases in plant growth,  
532 differentiation and development processes, in: Lobarzewski, J., Greppin, H., Penel, C.,

533 Gaspar, T.H. (Eds.), Biochemical, Molecular and physiological aspects of plant  
534 peroxidases. Université de Genève, pp. 249-280.

535 Ghosh, M., Bandyopadhyay, M., Mukherjee, A., 2010. Genotoxicity of titanium dioxide  
536 (TiO<sub>2</sub>) NPs at two trophic levels: plant and human lymphocytes. Chemosphere 81,  
537 1253-1262.

538 Giorgetti, E., Muniz Miranda, M., Caporali, S., Canton, P., Marsilia, P., Vergari, C.,  
539 Giammanco, F., 2014. TiO<sub>2</sub> nanoparticles obtained by laser ablation in water: Influence  
540 of pulse energy and duration on the crystalline phase. J. Alloy Compd. 643, S75-S79.

541 Giorgetti, L., Ruffini Castiglione, M., Bernabini, M., Geri, C., 2011. Nanoparticles effects on  
542 growth and differentiation in cell culture of carrot (*Daucus carota* L.). Agrochimica 55,  
543 45-53.

544 Giorgetti, L., Ruffini Castiglione, M., 2016. Oil palm *in vitro* regeneration:  
545 microdensitometric analysis during reproduction and development. Caryologia, on line  
546 first, DOI: 10.1080/00087114.2015.1109953

547 Gossett, D.R., Millhollon, E.P., Lucas, M.C., 1994. Antioxidant response to NaCl stress in  
548 salt-tolerant and salt-sensitive cultivars of cotton. Crop Sci. 34, 706-714.

549 Hartley-Whitaker, J., Ainsworth, G., Meharg, A.A., 2001. Copper- and arsenate-induced  
550 oxidative stress in *Holcus lanatus* L. clones with differential sensitivity. Plant Cell  
551 Environ. 24, 713-722.

552 Hotze, E.M., Phenrat, T., Lowry, G.V., 2010. Nanoparticle aggregation: challenges to  
553 understanding transport and reactivity in the environment. J. Environ. Qual. 39, 1909–  
554 1924

555 IARC - International Agency for Research on Cancer, 2010. Monographs 93. Titanium  
556 Dioxide. <http://monographs.iarc.fr/ENG/Monographs/vol93/mono93-7.pdf>

557 Jana, S., Choudhuri, M.A., 1982. Glycolate metabolism of three submerged aquatic  
558 angiosperm during aging. *Aquat. Bot.* 12, 345-354.

559 Jiang, H.S, Qiu, X.N., Li, G.B., Li, W., Yin, L.Y., 2014. Silver nanoparticles induced  
560 accumulation of reactive oxygen species and alteration of antioxidant systems in the  
561 aquatic plant *Spirodela polyrhiza*. *Environ. Toxicol. Chem.* 33, 1398-1405.

562 Kalyanasundharam, S., Prakash, M.J., 2015. Biosynthesis and characterization of titanium  
563 dioxide nanoparticles using *Pithecellobium dulce* and *Lagenaria siceraria* aqueous leaf  
564 extract and screening their free radical scavenging and antibacterial properties. *Int.*  
565 *Lett. Chem. Phys. Astron.* 50, 80-95.

566 Karnovsky, M.J., 1965. A formaldehyde-glutaraldehyde fixative of high osmolality for use  
567 in electron microscopy. *J. Cell Biol.* 27, 137-138.

568 Kaveh, R., Li, Y.S., Ranjbar, S., Tehrani, R., Brueck, C.L., Van Aken, B., 2013. Changes in  
569 *Arabidopsis thaliana* gene expression in response to silver nanoparticles and silver ions.  
570 *Environ. Sci. Technol.* 47, 10637-10644.

571 Kim, J.H., Lee, Y., Kim, E.J., Gu, S., Sohn, E.J., Seo, Y.S., An, H.J., Chang, Y.S., 2014.  
572 Exposure of iron nanoparticles to *Arabidopsis thaliana* enhances root elongation by  
573 triggering cell wall loosening. *Environ. Sci. Technol.* 48, 3477-3485.

574 Kováčik, J., Babula, P., Hedbavny, J., Švec, P., 2014. Manganese-induced oxidative stress  
575 in two ontogenetic stages of chamomile and amelioration by nitric oxide. *Plant Sci.*  
576 215-216, 1-10.

577 Kumari, M., Mukherjee, A., Chandrasekaran, N., 2009. Genotoxicity of silver  
578 nanoparticles in *Allium cepa*. *Sci. Total Environ.* 407, 5243-5246.

579 Kutik, J., Kuthanova, A., Smertenko, A., Fischer, L., Opatrny, Z., 2014. Cadmium-induced  
580 cell death in BY-2 cell structure starts with vacuolization of cytoplasm and terminates  
581 with necrosis. *Physiol. Plant.* 151, 423-433.



582 Larue, C., Laurette, J., Herlin-Boime, N., Khodja, H., Fayard, B., Flank, A.M., Brisset, F.,  
583 Carriere, M., 2012. Accumulation, translocation and impact of TiO<sub>2</sub> nanoparticles in  
584 wheat (*Triticum aestivum* spp.): influence of diameter and crystal phase. *Sci. Total*  
585 *Environ.* 431, 197-208.

586 Laware, S.L., Raskar, S., 2014. Effect of titanium dioxide nanoparticles on hydrolytic and  
587 antioxidant enzymes during seed germination in onion. *Int. J. Curr. Microbiol. Appl.*  
588 *Sci.* 3, 749-760.

589 Lepeduš, H., Jozić, M., Štolfa, I., Pavičić, N., Hackenbereger, K., Cesar, V., 2005. Changes  
590 in peroxidase activity in the peel of Unshiu Mandarin (*Citrus unshiu* Marc.) fruit with  
591 different storage treatments. *Food Technol. Biotech.* 43, 71-77.

592 Liu, W.K., 2011. TiO<sub>2</sub>-NPs application in agriculture: a review, in Hendriks, B.P. (Ed.),  
593 *Agricultural research updates*. Nova Publisher, Hauppauge, New York, pp. 137-145.

594 Ma, X., Geiser-Lee, J., Deng, Y., Kolmakov, A., 2010. Interactions between engineered  
595 nanoparticles (ENPs) and plants: Phytotoxicity, uptake and accumulation. *Sci. Total*  
596 *Environ.* 408, 3053-3061.

597 Mittler, R., 2002. Oxidative stress, antioxidants and stress tolerance. *Trends Plant Sci.* 7,  
598 405-410.

599 Mohammadi, R., Maali-Amiri, R., Mantri, N.L., 2014. Effect of TiO<sub>2</sub> nanoparticles on  
600 oxidative damage and antioxidant defense systems in chickpea seedlings during cold  
601 stress. *Russ. J. Plant Physiol.* 61, 768-775.

602 Moreno-Olivas, F., Gant Jr., V.U., Johnson, K.L., Peralta-Videa, J.R., Gardea-Torresdey,  
603 J.L., 2014. Random amplified polymorphic DNA reveals that TiO<sub>2</sub> nanoparticles are  
604 genotoxic to *Cucurbita pepo*. *J. Zhejiang Univ.-SCI. A* 15, 618-623.

605 Moura, J.C.M.S., Bonine, C.A.V., de Oliveira Fernandes Viana, J., Carnier Dornelas, M.,  
606 Mazzafera, P., 2010. Abiotic and biotic stresses and changes in the lignin content and

607 composition in plants. J. Integr. Plant Biol. 52, 360-376.

608 Nakano, Y., Asada, K., 1981. Hydrogen peroxide is scavenged by ascorbate-specific  
609 peroxidase in spinach chloroplasts. Plant Cell Physiol. 22, 867-880.

610 Navari-Izzo, F., Meneguzzo, S., Loggini, B., Vazzana, C., Sgherri, C.L.M., 1997. The role  
611 of the glutathione system during dehydration of *Boea hygroskopica*. Physiol. Plant. 99,  
612 23-30.

613 Navarro, E., Baun, A., Behra, R., Hartmann, N.B., Filser, J., Miao, A.J., Quigg, A.,  
614 Santschi, P.H., Sigg, L., 2008. Environmental behavior and ecotoxicity of engineered  
615 nanoparticles to algae, plants, and fungi. Ecotoxicology 17, 372-386.

616 Ortlieb, M., 2010. White giant or white Dwarf? Particle size distribution measurements of  
617 TiO<sub>2</sub>. GIT Lab. J. Eur. 14, 42-43.

618 Pakrashi, S., Jain, N., Dalai, S., Jayakumar, J., Chandrasekaran, P.T., Raichur, A.M.,  
619 Chandrasekaran, N., Mukherjee, A., 2014. *In vivo* genotoxicity assessment of titanium  
620 dioxide nanoparticles by *Allium cepa* root tip assay at high exposure concentrations.  
621 Plos One 9, e87789.

622 Parida, A.K., Das, A.B., 2005. Salt tolerance and salinity effects on plants: a review.  
623 Ecotox. Environ. Safety 60, 324-349.

624 Planchet, P., Kaiser, W.M., 2006. Nitric oxide production in plants. Plant. Signal. Behav. 1,  
625 46-51.

626 Poborilova, Z., Opatrilova, R., Babula, P., 2013. Toxicity of aluminium oxide nanoparticles  
627 demonstrated using a BY-2 plant cell suspension culture model. Environ. Exp. Bot. 91, 1-  
628 11.

629 Praetorius, A., Scheringer, M., Hungerbühler, K., 2012. Development of environmental fate  
630 models for engineered nanoparticles: a case study of TiO<sub>2</sub> nanoparticles in the Rhine  
631 river. Environ. Sci. Technol. 46, 6705-6713.

632 Raliya, R., Biswas, P., Tarafdar, J.C., 2015. TiO<sub>2</sub> nanoparticle biosynthesis and its  
633 physiological effect on mung bean (*Vigna radiata* L.). *Biotech. Rep.* 5, 22-26.

634 Ruffini Castiglione, M., Cremonini, R., 2009. Nanoparticles and higher plants. *Caryologia* 62,  
635 161-165.

636 Ruffini Castiglione, M., Giorgetti, L., Cremonini, R., Bottega, S., Spanò, C., 2014. Impact  
637 of TiO<sub>2</sub> nanoparticles on *Vicia narbonensis* L.: potential toxicity effects. *Protoplasma*  
638 251, 1471-1479.

639 Ruffini Castiglione, M., Giorgetti, L., Geri, C., Cremonini, R., 2011. The effects of nano-  
640 TiO<sub>2</sub> on seed germination, development and mitosis of root tip cells of *Vicia*  
641 *narbonensis* L. and *Zea mays* L. *J. Nanopart. Res.* 13, 2443-2449.

642 Seeger, E.M., Buan, A., Kästner, M., Trapp, S., 2009. Insignificant acute toxicity of TiO<sub>2</sub>  
643 NPs to willow trees. *J. Soils Sediments* 9, 46-53.

644 Sharma, P., Bhatt, D., Zaidi, M.G.H., Saradhi, P.P., Khanna, P.K., Arora, S., 2012. Silver  
645 nanoparticle-mediated enhancement in growth and antioxidant status of *Brassica*  
646 *juncea*. *Appl. Biochem. Biotechnol.* 167, 2225-2233.

647 Song, U., Shin, M., Lee, G., Roh, J., Kim, Y., Lee, E.J., 2013. Functional analysis of TiO<sub>2</sub>  
648 nanoparticle toxicity in three plant species. *Biol. Trace Elem. Res.* 155, 93-103.

649 Spanò, C., Bottega, S., Lorenzi, R., Grilli, I., 2011. Ageing in embryos from wheat grains  
650 stored at different temperatures: oxidative stress and antioxidant response. *Funct. Plant*  
651 *Biol.* 38, 624-631.

652 Spanò, C., Bruno, M., Bottega, S., 2013. *Calystegia soldanella*: dune versus laboratory  
653 plants to highlight key adaptive physiological traits. *Acta Physiol. Plant.* 35, 1329-  
654 1336.

655 Shukla, R.K., Kumar, A., Gurbani, D., Pandey, A.K., Singh, S., Dhawan, A., 2013. TiO<sub>2</sub>  
656 nanoparticles induce oxidative DNA damage and apoptosis in human liver cells.  
657 Nanotoxicology 7, 48-60.

658 USEPA (U.S. Environ Protection Agency), 2010. Emerging contaminants-nanomaterials.  
659 [http://www.epa.gov/region9/mediacenter/nano-ucla/emerging\\_contaminant\\_nanomaterials.pdf](http://www.epa.gov/region9/mediacenter/nano-ucla/emerging_contaminant_nanomaterials.pdf)

660 Zhao, L., Peng, B., Hernandez-Viezcas, J.A., Rico, C., Sun, Y., Peralta-Videa, J.R., Tang,  
661 X., Niu, L., Jin, L., Varela-Ramirez, A., Zhang, J., Gardea-Torresdey, J.L., 2012. Stress  
662 response and tolerance of *Zea mays* to CeO<sub>2</sub> nanoparticles: cross talk among H<sub>2</sub>O<sub>2</sub>, heat  
663 shock protein, and lipid peroxidation. ACS Nano 6, 9615-9622.

664 Zheng, L., Hong, F., Lu, S., Liu, C., 2005. Effect of TiO<sub>2</sub>-NPs on strength of naturally aged  
665 seeds and growth of spinach. Biol Trace Elem Res 104, 83-92.

666

667 **Figure captions**

668

669 **Fig. 1.** *V. faba* seedlings. Representative samples after 72h germination in water (control), in  
670 the presence of 50mg/L of TiO<sub>2</sub> P-NPs, S-NPs and bulk counterpart (Bulk).

671

672 **Fig. 2.** TEM images of (a) P-NPs (arrows) and (b) S-NPs (arrows). (c) Cell portion of control  
673 *V. faba* root. The arrow indicates rough endoplasmic reticulum. (d, e) Cell portions of P-NPs  
674 treated roots. The arrows indicate P-NPs. (f) P-NPs in two rhizodermis cell walls (arrows). c,  
675 chromatin; m, mitochondria; n, nucleolus; v, vacuole; w, rhizodermis cell wall.

676

677 **Fig. 3.** TEM images of (a) aggregate of NPs (arrows) in the vacuole of S-NPs treated root  
678 cell. (b) S-NPs (arrows) in portion of degenerated cytoplasm. The double arrows indicate  
679 vesicles with rough membranes; the arrowheads indicate vesicles. (c) Aggregates of S-NPs  
680 (arrows) in the rhizodermis cell wall. (d-f) Portions of cells of B treated roots. The arrows  
681 indicate smooth endoplasmic reticulum. n, nucleus; dc, degenerated cytoplasm; o, not well  
682 recognizable organelles; b, weakly electron opaque bodies; w, rhizodermis cell wall.

683

684 **Fig. 4.** Different behaviour of *V. faba* root apex. Mean values of mitotic index (MI %),  
685 aberration index (AI %) and of micronuclei frequency (MNC %) recorded after 72h  
686 germination in water (control), in the presence of 50mg/L of TiO<sub>2</sub> P-NPs, S-NPs and bulk  
687 counterpart (Bulk). Bars represent standard errors. Different letters, within each analyzed  
688 parameter, indicate significant differences by Bonferroni's multiple comparison test ( $p <$   
689 0.05).

690

691 **Fig. 5.** Representative mitotic abnormalities in TiO<sub>2</sub> S-NPs and Bulk treatments in *V. faba* root  
692 tip meristem. (a) Micronuclei; (b-c) sticky chromosomes; (d) laggard chromosome in early  
693 anaphase; (e-f) C metaphases; (g) somatic pairing; (h-i) reduction grouping; (j) laggard  
694 chromosome in disturbed anaphase; (k-m) chromosome bridges in anaphases.

695

696 **Fig. 6.** Cross hand sections of *V. faba* roots of seedlings after 72h germination in water  
697 (control), in the presence of 50mg/L of TiO<sub>2</sub> P-NPs, S-NPs and bulk counterpart (Bulk).

698 The plate comprehends representative images of *in situ* detection of H<sub>2</sub>O<sub>2</sub>, of reactive nitrogen  
699 species (RNS), lipid peroxidation (Lipid perox) and peroxidase activity (POD activity). Bars  
700 indicate 200  $\mu$ m.

701

702 **Table 1.** Growth and physiological parameters in *Vicia faba* roots of seedlings after 72h of  
 703 germination in water (control), in the presence of TiO<sub>2</sub> Plasma Tech (P-NPs), Sigma (S-NPs) and  
 704 bulk counterpart (Bulk). Relative water content (RWC), thiobarbituric acid reactive substances  
 705 (TBARS), total ascorbate (reduced ascorbate, ASA + dehydroascorbate, DHA), total glutathione  
 706 (reduced form, GSH + oxidised form, GSSG), ascorbate peroxidase (APX), glutathione peroxidase  
 707 (GPX), guaiacol peroxidase (POD) and catalase (CAT).

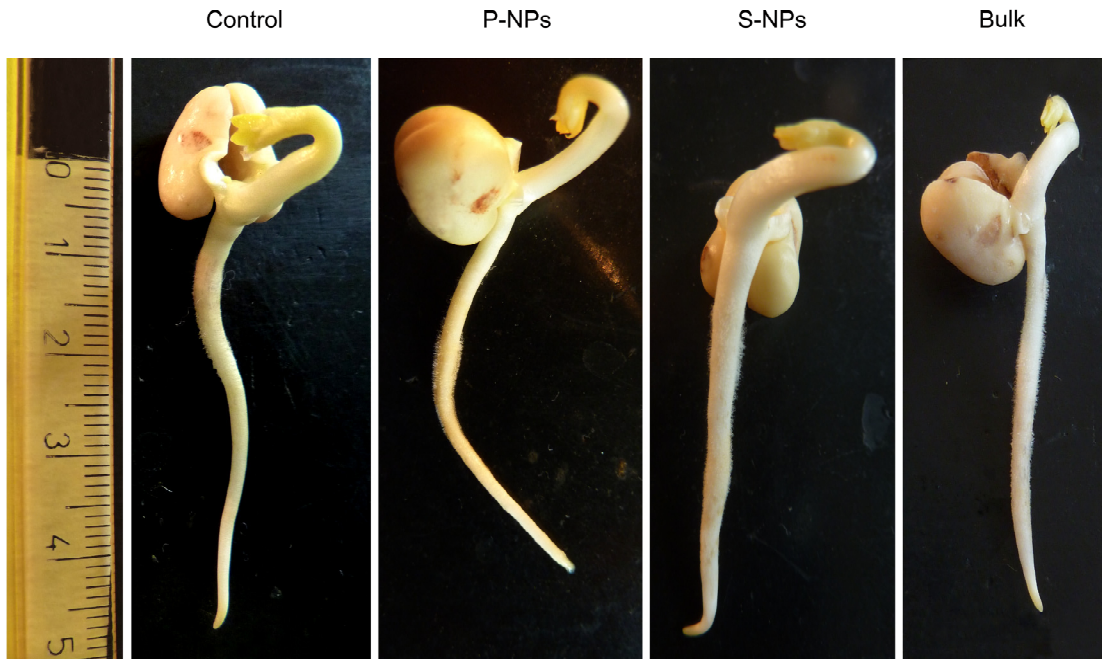
708

	Control	Bulk	TiO <sub>2</sub> P-NPs	TiO <sub>2</sub> S-NPs
Germination (%)	86.67±4.25a	86.67±2.04a	91.67±3.73a	89.58±2.08a
Root length (mm)	46.62±1.41ab	41.81±1.78b	48.16±1.30a	44.37±1.68ab
Vigour Index	4079.17±76.40b	3696.67±44.10c	4392.59±50.17a	3975.00±28.79b
Water content (%)	94.33±0.13ab	94.77±0.35a	93.13±0.38b	93.70±0.35ab
RWC (%)	89.73±1.04b	94.36±1.80a	84.67±0.52c	88.00±1.76bc
H <sub>2</sub> O <sub>2</sub> (µmol g <sup>-1</sup> DW)	70.06±2.42b	91.43±1.49a	38.95±1.51d	49.21±2.55c
TBARS (nmol g <sup>-1</sup> DW)	259.34±19.15b	388.38±7.91a	247.54±25.31b	278.83±5.28b
Proline (µmol g <sup>-1</sup> DW)	78.64±2.14a	53.29±1.54b	44.19±1.63c	38.63±3.67c
Total ascorbate (µmol g <sup>-1</sup> DW)	108.68±1.08b	128.23±3.01a	97.54±1.33c	106.90±0.37b
ASA/DHA	1.10±0.03c	0.97±0.05c	1.60±0.05b	1.79±0.04a
Total glutathione (µmol g <sup>-1</sup> DW)	1.22±0.06b	1.43±0.05a	0.97±0.06c	1.09±0.02bc
GSH/GSSG	2.53±0.27b	1.71±0.13b	5.81±0.74a	2.01±0.13b
APX (U g <sup>-1</sup> protein)	606.60±7.40a	510.27±18.17b	500.63±7.92b	510.80±20.51b
GPX (U g <sup>-1</sup> protein)	1196.67±11.87a	1037.30±8.45a	1032.57±34.03a	1022.02±67.67a
POD (U g <sup>-1</sup> protein)	1522.02±38.60c	1647.61±34.12b	1415.27±16.42d	2239.91±20.73a
CAT (U g <sup>-1</sup> protein)	5049.53±487.63a	3832.88±387.16b	2649.43±131.83b	3031.52±282.09b

709

710 Data are the mean of at least three replicates ± SE. Means followed by the same letters within the same row are not  
 711 significantly different at 1%.

712



713

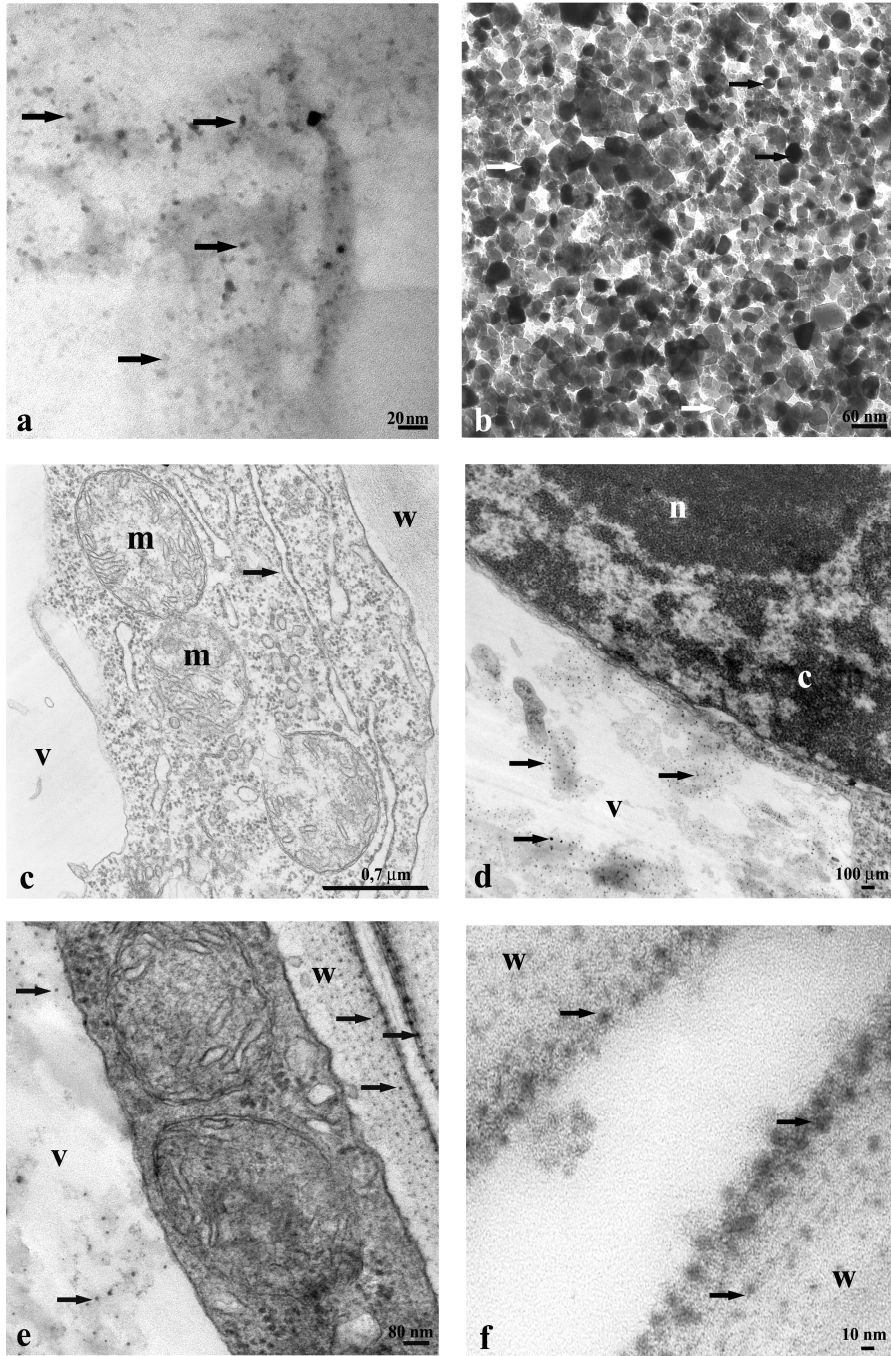
714 Figure 1

715

716

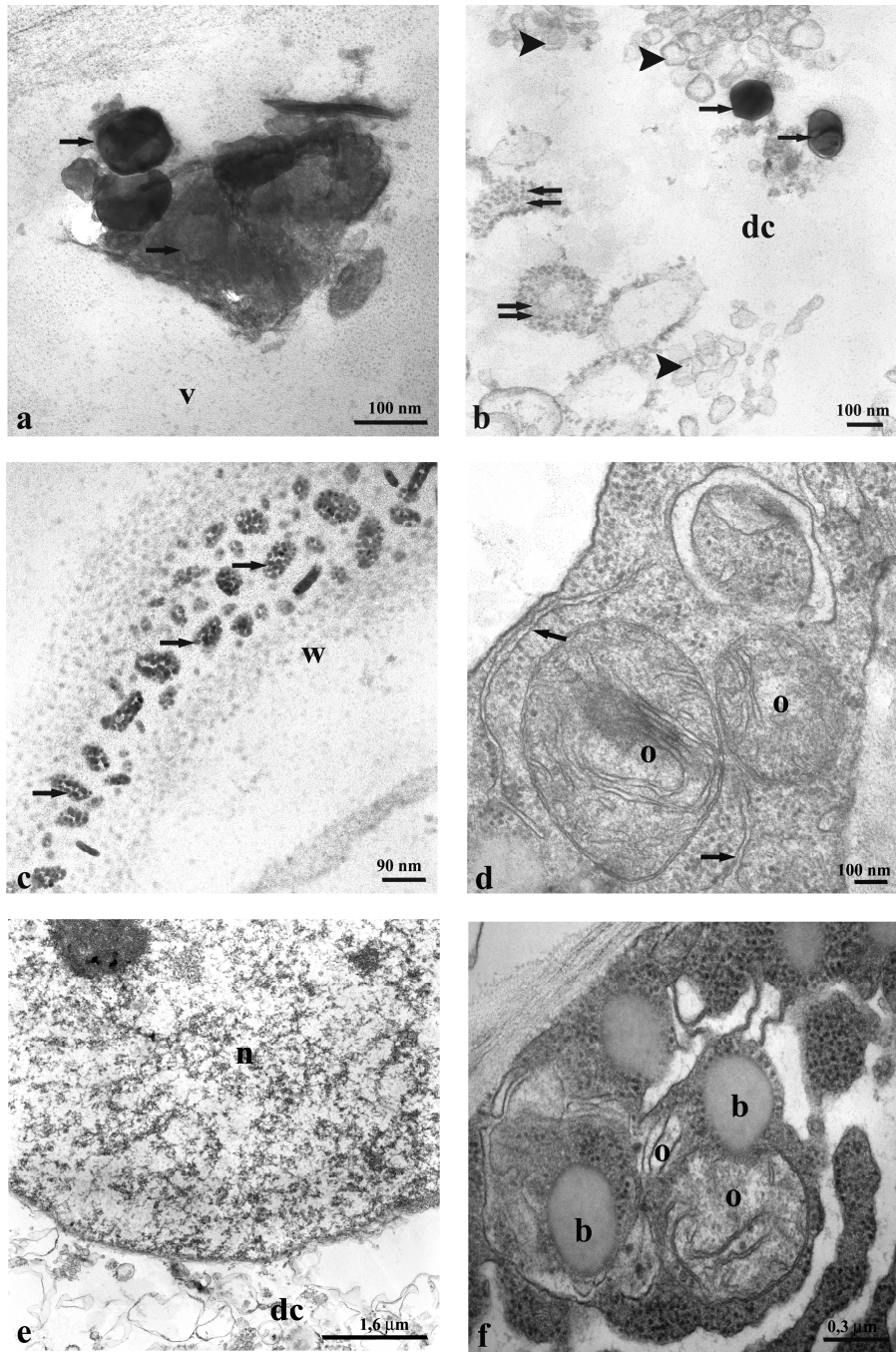
717

718



719  
 720 Figure 2  
 721  
 722



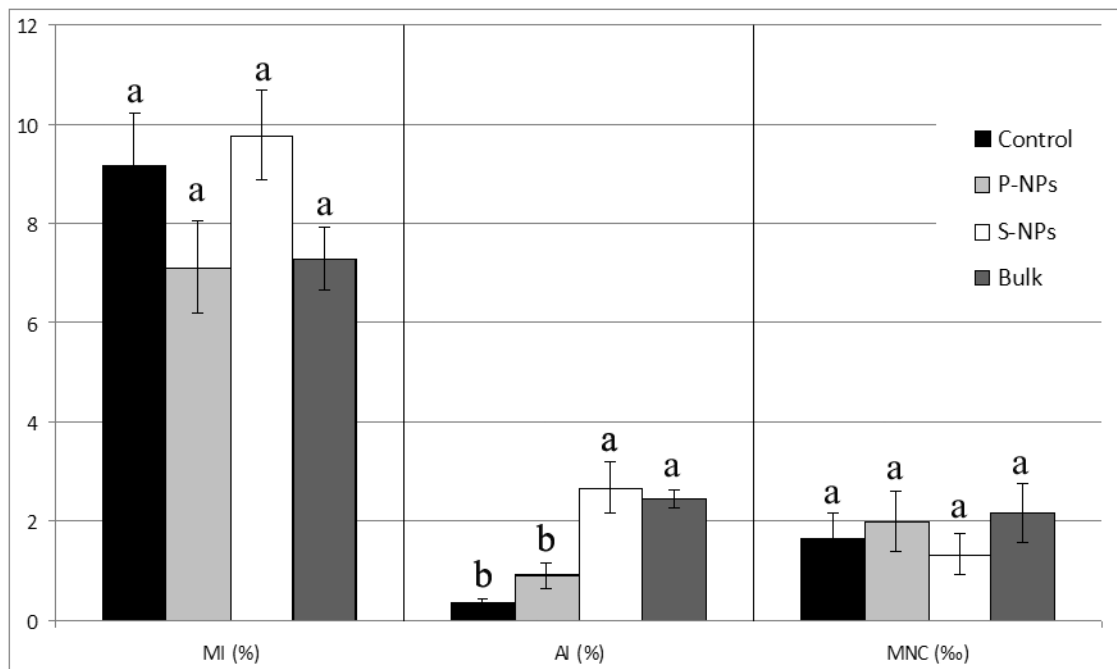


723  
 724 Figure 3  
 725  
 726

727

728

729



730

731 Figure 4

732

733

734

735

736

737

738

739

740

741

742

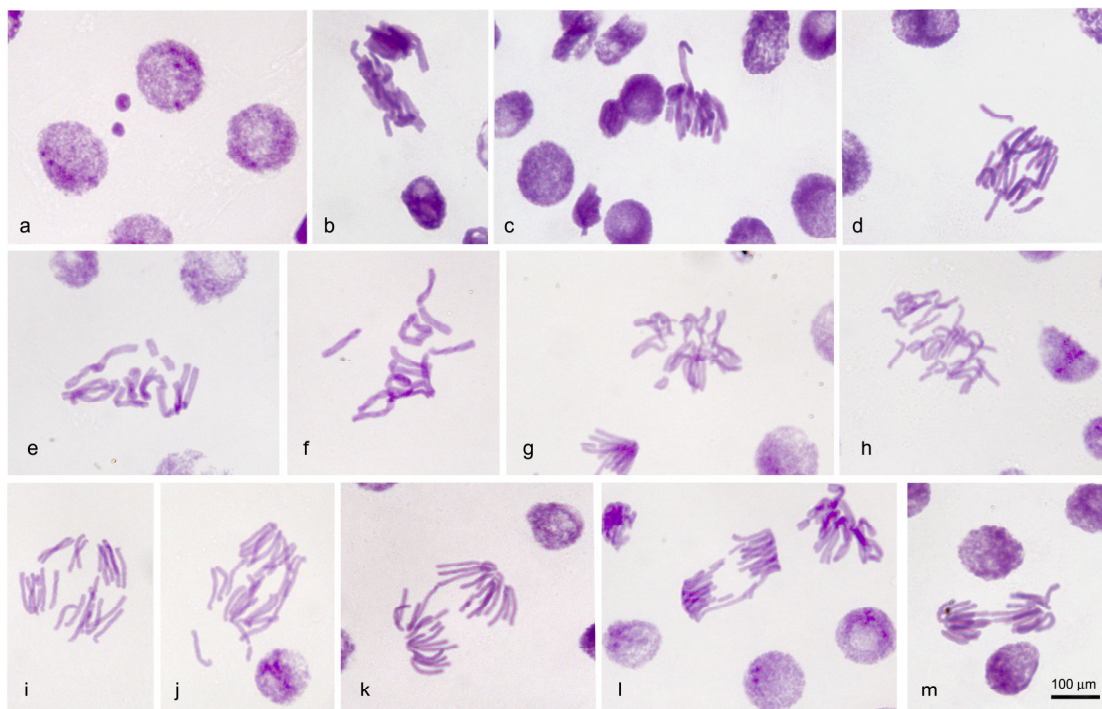
743

744

745

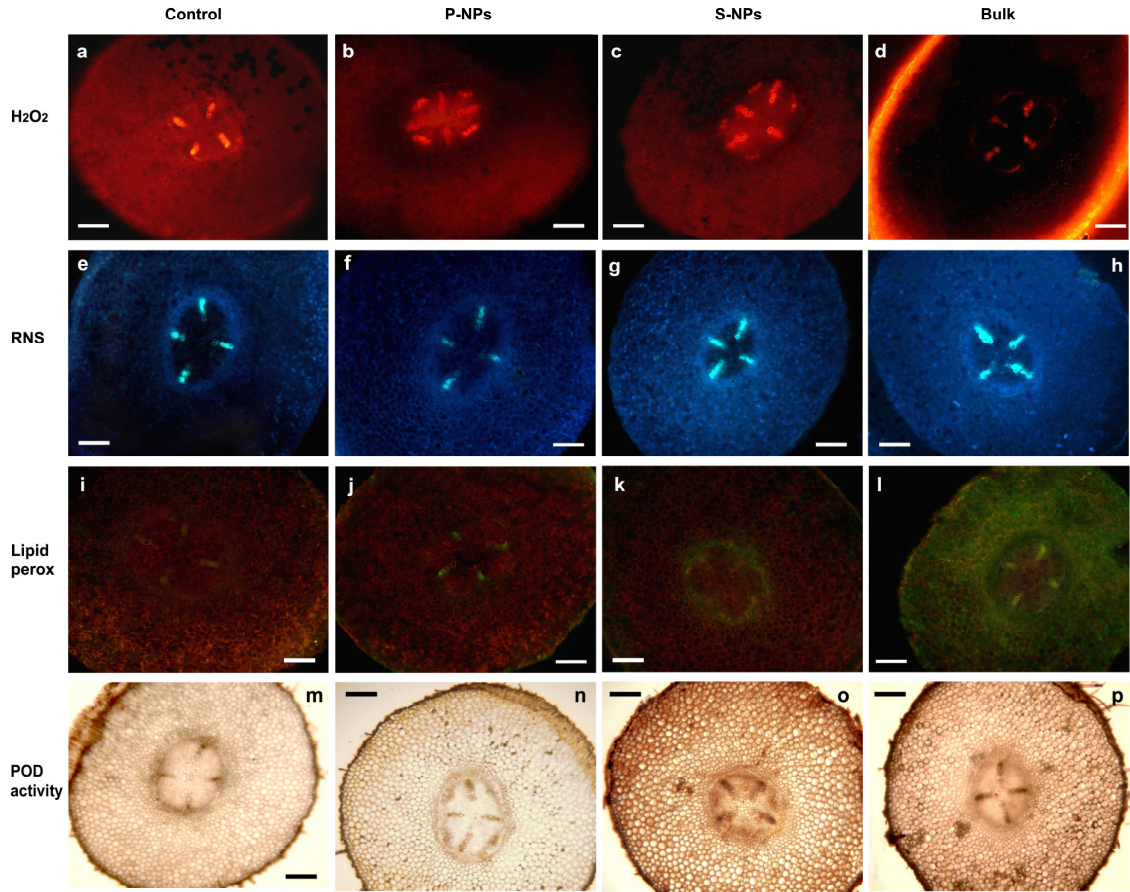
746

747



748  
749 Figure 5

750  
751  
752  
753  
754  
755  
756  
757  
758  
759  
760  
761  
762  
763  
764  
765  
766  
767



768

769 Figure 6

770

771

772

773

774

775

776

777

778

779

780

781

782

783

784  
785  
786  
787  
788  
789  
790  
791  
792  
793  
794  
795  
796  
797